SECOND EUROPEAN CONFERENCE ON EARTHQUAKE ENGINEERING AND SEISMOLOGY, ISTANBUL AUG. 25-29, 2014

EFFECT OF MODELLING MASS AND DAMPING ON THE PREDICTION OF AXIAL FORCE VARIATION IN CANTILEVER WALLS DURING NON-LINEAR RESPONSE ANALYSIS

Alfredo GONZÁLEZ FONSECA[1], Enrico SPACONE[2] and Roberto NASCIMBENE[3]

The axial load in cantilever walls does not remain constant, under certain circumstances, during numerically simulated non-linear earthquake response analyses. This happens even when obvious sources of axial load variation such as shear from coupling beams and vertical input are not included (González 2013). An increase in axial load may lead to an increase in base shear demand, while a decrease may result in greater curvature demands. Paragraphs 5.4.2.5(3) *et seq.* in Eurocode 8-1 (EN 1998-1:2003) acknowledge the development of dynamic axial forces in walls and require that it be considered during analysis and design, suggesting plus or minus 50% of the gravity loads if more detailed calculations are not available.

This paper reports the insight gained into the nature of this phenomenon through an extensive campaign of numerical analyses. The dynamic variation in axial load (ΔN) in cantilever walls stems from the rocking-like motion of the wall itself, which generates damping and inertia forces (ΔN_D and ΔN_I, respectively) in the walls' axial direction. The results show that ΔN_I is a true physical phenomenon while ΔN_D derives entirely from the way damping is idealized in the available numerical response analysis techniques. It follows that the analyst should aim at minimizing the latter while properly predicting the former. The results also suggest that ΔN_I is already accounted for by several available models, making the 50% increase suggested by Eurocode redundant. Both phenomena are quantified and discussed in detail. They are further discussed from the point of view of the influence of modelling decisions on the accuracy of the predicted response and on the subsequent design process.

1. Introduction

The axial load in cantilever walls does not remain constant, under certain circumstances, during simulated non-linear earthquake response analyses (González, 2013; Correia, Almeida, & Pinho, 2013). This paper addresses the following questions: To what extent does the axial force variation correspond to an actual physical phenomenon? To what extent is it a numerical effect? And: How relevant is it to the design of safe structures?

Flexural cracks open in the plastic hinge region at the base of cantilever walls during cyclic non-linear responses. The neutral axis moves away from the geometric centre because of the cracking, which leads to an elongation of the element along its geometric axis. The cracks close back and then open again on the opposite wall side as the cycle reverses, while the neutral axis also reverses position leading again to element elongation. The reinforcement eventually undergoes inelastic deformation and does not return to its original length as the cracks close, leading to some cumulative residual elongation of

[1] PhD candidate, ROSE Programme, UME School/IUSS, Pavia, Italy, alfredo.gonzalez@umeschool.it
[2] Chair, Dept. of Engineering and Geology, University of Chieti-Pescara, Pescara, Italy, espacone@unich.it
[3] Head of Structural Analysis, European Centre for Training and Research in Earthquake Engineering (EUCENTRE), Pavia, Italy, roberto.nascimbene@eucentre.it

the element. This cyclic elongation implies that the masses directly or indirectly attached will experience a cyclic vertical motion. Something very similar happens in rocking walls such as precast-posttensioned elements where dry joints – rather than smeared cracks – open. For this reason, this phenomenon is hereafter referred to as *rocking like motion.*

The axial load in walls can fluctuate from its static value (due to the gravity loads) during numerically simulated earthquake response through the combined effects of:

a) Dynamic response of the vertical mass-wall subsystem and the vertical mass-floor beams subsystem (in the absence of vertical seismic input) through excitation and coupling provided by the *rocking-like motion*;
b) Dynamic response of the dashpot through which damping is modelled, again through coupling of the involved degrees of freedom due to the *rocking-like motion*;
c) Vertical seismic input which excites the vertical mass and dashpots.

The first effect will show only if a vertical mass is modelled regardless of the level of damping; it is referred to here as *mass effect*. The second will show whenever damping is modelled and its relative importance depends greatly on the type and level of damping chosen for the model; it is here referred to as *damping effect*. The effect of vertical seismic input requires that the models explicitly incorporate both a vertical component of the input acceleration history and the vertical component of the nodal masses. This paper focuses on the effects of mass and damping and its implications for the prediction of the seismic response of wall systems. The effects of vertical ground motion will be the subject of forthcoming research and will be reported in future publications.

The phenomena of interest are only captured by models that reproduce the *rocking-like motion* and the translation of the neutral axis. These models include those in which the wall itself is represented through distributed-plasticity frame elements with fibre sections and those in which plasticity is lumped at expected hinge locations in a multi-spring phenomenological model. Conversely, this effect cannot be captured when inelastic behaviour is modelled through a phenomenological lumped-plasticity approach in which the plastic hinge at the base of the wall is simulated through a non-linear rotational spring, because this type of model cannot reproduce the *rocking-like motion* and the translation of the neutral axis. In addition, these models cannot reproduce the axial force-moment interaction and thus any variation in axial force would have no influence on the response.

An increased axial force can mean larger moment capacity and thus larger base shear at over-strength, which the design needs to account for. On the other hand, a reduction in axial force close to peak displacement demand reduces the moment capacity. Such a reduction can lead to premature failure of the reinforcement and subsequently greater displacement ductility demand than intended during design. It is for these reasons that paragraphs 5.4.2.5(3) *et seq.* in Eurocode 8-1 (EN 1998-1:2003) acknowledge the development of dynamic axial forces in walls and require that it be considered during analysis and design, suggesting plus or minus 50% of the gravity loads if more detailed calculations are not available.

2. Evidence of axial load variation

A very simple non-linear 'stick' model (described in the next section and shown in Figure 3a) readily shows the phenomenon in question. A ground motion described in section 3 is applied to four versions of the model resulting from the combination of low (0.1%≈0%) and moderate (2%) damping, and a vertical mass which is either zero or equal to the horizontal mass. The system responds well into the non-linear range. There are six masses and the reinforced concrete wall is modelled with force-based fibre-section frame elements. Damping is tangent-stiffness-proportional. Figure 1 shows an array of plots of axial force vs time for these four cases. While there is nearly no variability in axial load for an undamped system without vertical mass, this variability is significant when damping and vertical masses are considered, leading to a fourfold of the static value at one instant and net tension in the next.

The effects on the moment-curvature response are evident from Figure 2 where the predictions with and without vertical mass are compared: jagged loops which do not match the predicted curves, increased moment capacity at over-strength, premature failure of the rebar and increased curvature demand appear in the response of the model with vertical mass.

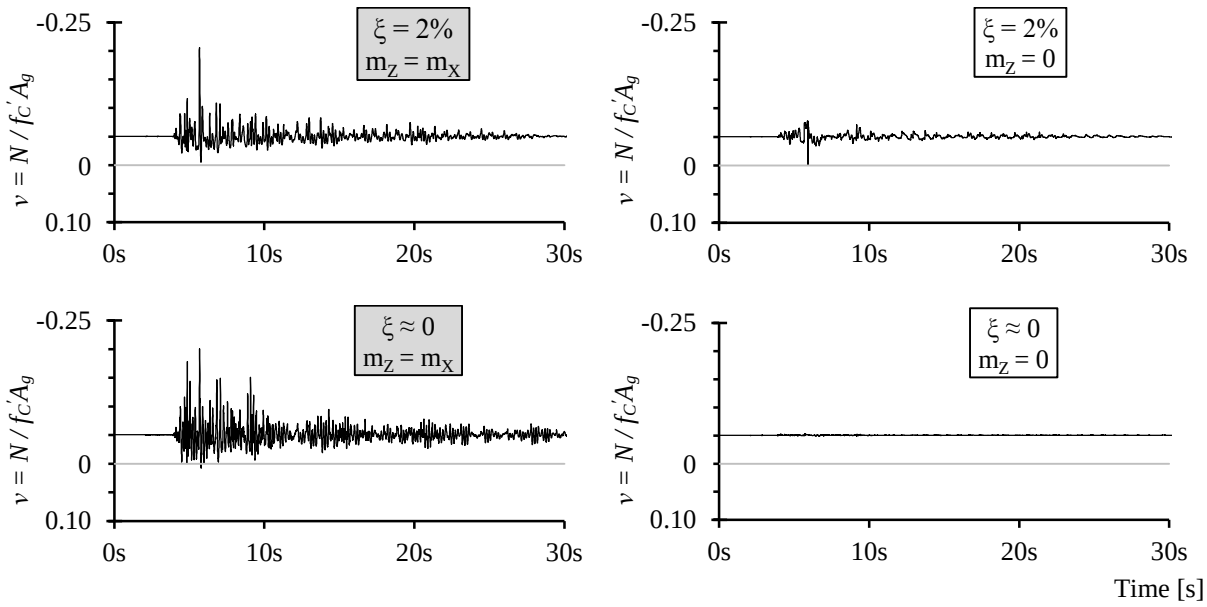

Figure 1. History of normalised axial force in a shear wall (model S) in response to horizontal ground motion.

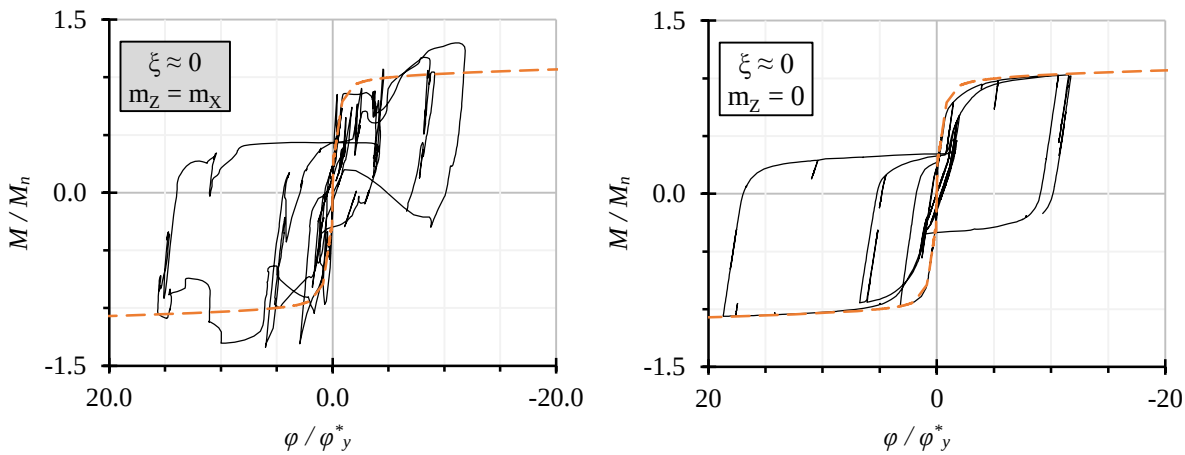

Figure 2. Normalised moment-curvature response at the wall base (model S) to the same horizontal ground motion with and without vertical mass. Shown dashed is the pushover curve. *Note:* $\varphi^*_y = \varphi_y M_n / M_y$

3. Models and input ground motions for *nlth* analysis

This study uses three models (shown in Figure 3) with different degrees of complexity for non-linear time history (*nlth*) analysis, labelled "S", "P" and "F". Model "S" is a vertical stick with 6 mass nodes (*i.e.*, *n*=6) used for section 4. Model "P" is an inverted pendulum with one equivalent force-based fibre-section frame element ("*fbfe*") for the wall and one equivalent mass node. Model "F" uses a single equivalent *fbfe* for the wall and a subsystem for the floors comprised of elastic beams and lumped masses (*n*=5). In all cases, the wall is represented by non-linear force-based fibre-section frame elements with 5 Gauss-Lobatto integration points (IPs). The beam elements representing the floors in model F are linear and the beam end not supported on the wall is supported on a spring with a vertical stiffness similar to that of the wall and free to move horizontally. Their out-of-plane stiffness is changed as required by the analysis objectives to model different floor characteristics. They are not intended to model a flexible floor diaphragm (in the in-plane direction) as this is not part of the current investigation.

Damping is modelled using tangent-stiffness-proportional damping (*tspd*). This is a common choice for *nlth* analyses to overcome some of the drawbacks of the classical Rayleigh damping (Priestley & Grant, 2005; Petrini, Maggi, Priestley, & Calvi, 2008).

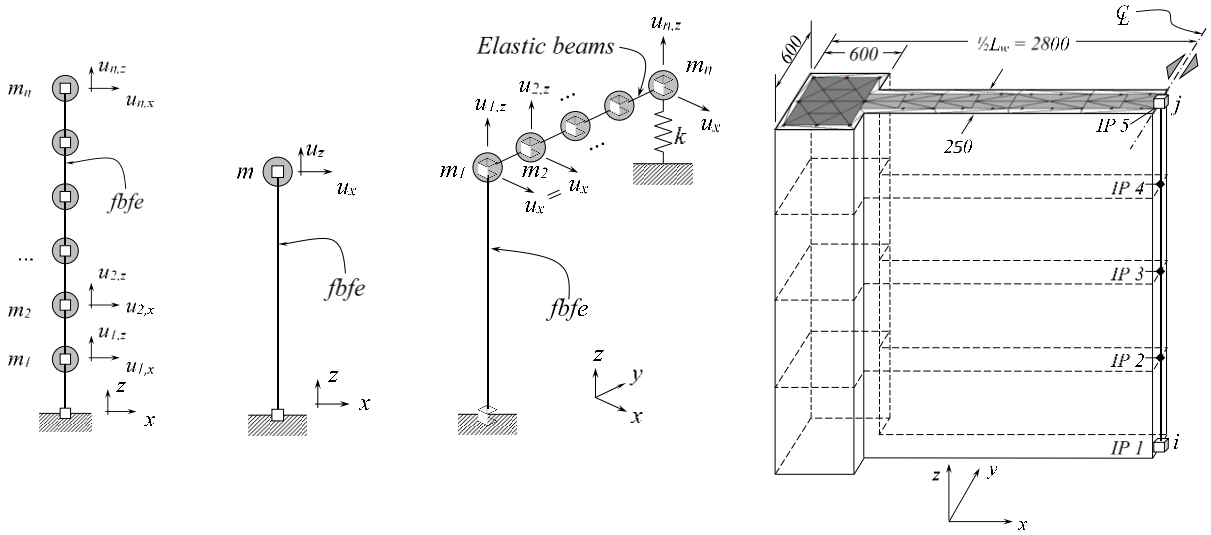

(a) Stick 2D ("S") model

(b) Inverted pendulum 2D ("P") model

(c) MDOF 3D floor ("F") model

(d) *fbfe* section discretization and integration points (*IP 1~5*)

Figure 3. Models used for *nlth* analyses

Table 1. Modelling parameters

Parameter	Model type ID								
	S			P			F		
Degrees of freedom	u_X	u_Z	θ_Y	u_X	u_Z	θ_Y	u_X	u_Z	θ_Y
Kinematic	6	6	6	1	2	1	1	5	1
Dynamic	6	6	—	1	1	—	1	5	—
Masses [ton]	250	$\begin{cases}250\\0\end{cases}$	—	1500	0~3000	—	1565(1)	1565(1)	—
Elastic beam elements									
Stiffness EI_{xx} [kNm^2]	—			—			$6\cdot10^5 \sim 2.6\cdot10^{12}$		
Length $L^{(2)}$ [m]	—			—			8 (h=2)		
Vertical spring k [kN/m]	—			—			$5.04\cdot10^6$		
Fibre elements									
Length $L^{(2)}$ [m]	21.5 (h_1=4, $h_{2..6}$=3.5)			15 (=h)			15 (=h)		
Integration points (IPs)	5			5			5		
Length of first IP(3) [m]	0.69			5.175			5.175		
No of fibres	200			200			200		
Longitudinal reinforcement	Edges: 8ø25 (1.1%), Web: 36ø16 (0.66%)								

Notes: (1) The lumped masses in model F are not all equal: m_1=246, $m_{2..4}$=293, m_5 = 440 [ton]
(2) h is the length of the discrete element (mesh size)
(3) Integration points are located at χ = (-1, -.655, 0, .655, 1)·L/2 measured from mid span of the element

The vertical masses are set to zero in selected runs in order to isolate the effect of damping from the effects of mass. In other runs the vertical masses are set equal to the horizontal masses, and in one set of runs the vertical masses changes while keeping the horizontal masses constant. Throughout the figures in this paper, hollow (white) markers represent data points for the cases without vertical mass, while full (grey) markers represent those cases that include the vertical mass.

The ground motion used is the unscaled fault-normal component of the Rio Dell Overpass record of the Cape Mendocino, California earthquake of April 25, 1992. It was selected because it closely matches the reference spectrum (Eurocode 8 Type 1 Soil class C with PGA=0.345g) in the range of periods relevant to the first-mode lateral response (0.6s to 1.8s). This choice is arbitrary but consistent with the hazard appropriate for the design of a normal structure in a region of high seismicity.

The fibre concrete and steel material properties are shown in Figure 4 and the most relevant modelling parameters are summarized in Table 1 for the three models shown in Figure 3. Geometric non-linearity was taken into account in all cases. The Hilber-Huges-Taylor method was used, with α=-0.1, β=0.3025, γ=0.6. The constraints were enforced through penalty functions (Felippa, 2013) with weights 10^{10}.

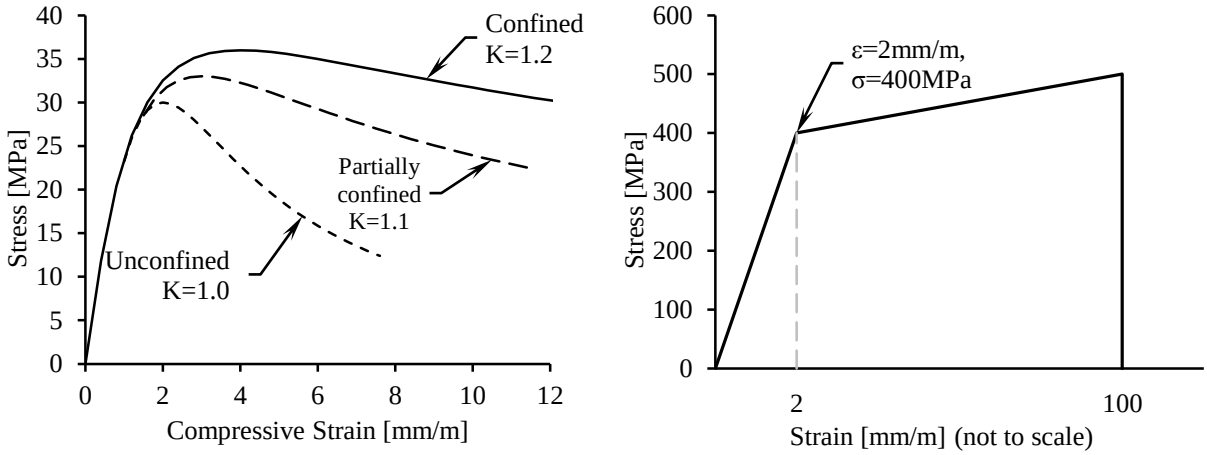

Figure 4. Material stress-strain relationships (left: concrete, right: steel)

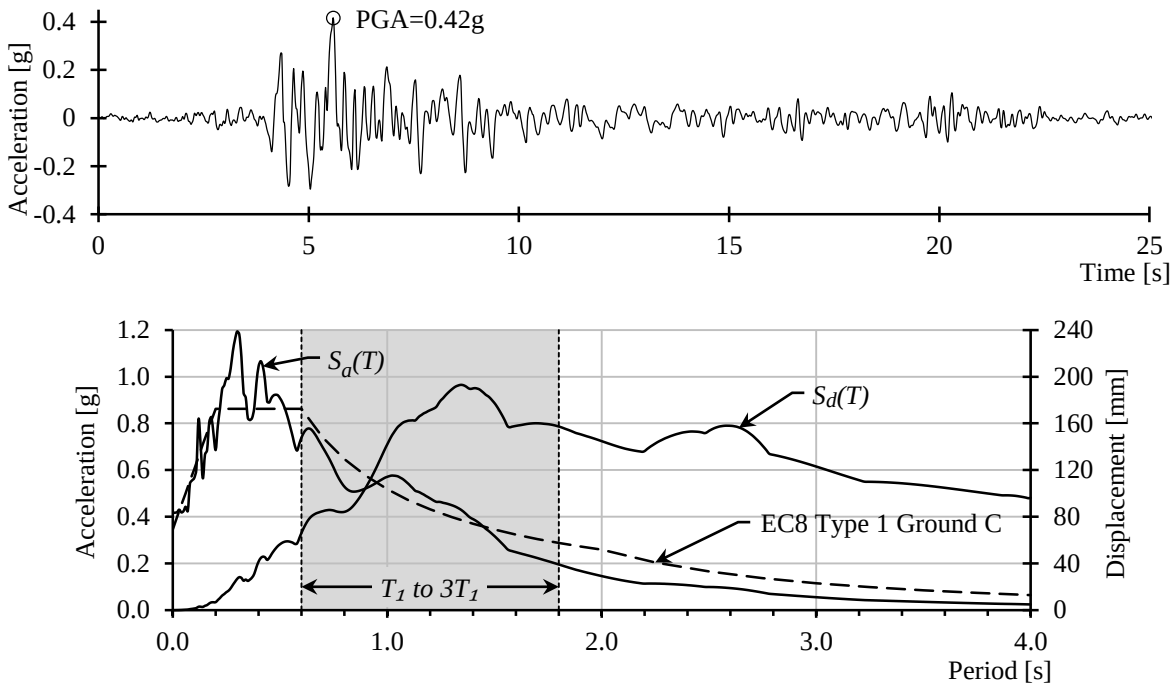

Figure 5. Input ground motion (top) and its acceleration (Sa) and displacement (Sd) response spectra (bottom). The EC8 type 1 ground C spectrum is shown dashed as a reference. The shaded area represents the range of first-mode periods expected during non-linear response.

4. Influence of damping

Overview of initial stiffness-proportional damping

Classical Rayleigh damping is a convenient way of modelling damping in structures. It leads to an orthogonal damping matrix which allows for the modal decoupling of the equations of motion. The *proportional* damping matrix is calculated as

$$\boldsymbol{C} = a_M \boldsymbol{M} + a_K \boldsymbol{K}, \tag{1}$$

where $\boldsymbol{C}$, $\boldsymbol{M}$ and $\boldsymbol{K}$ are the damping, mass and initial stiffness matrices and a_K and a_M are constant coefficients. The two terms on the right-hand side of (1) are commonly referred to as the *mass-proportional* and the *stiffness-proportiona* terms, respectively. The damping ratio ξ_i for any mode i with period T_i can be shown to be

$$\xi_i = a_M T_i \frac{1}{4\pi} + a_K \pi T_i^{-1} \tag{2}$$

The coefficients a_K and a_M can be selected by the analyst to provide the required damping at any two periods while for any other period the damping is given by (2).

Several researchers (notably Bernal (1994), Priestley & Grant (2005) and Hall (2006)) have pointed out problems with classical Rayleigh damping when modelling non-linear response and short period structures. Alipour and Zareian (2008) and Charney (2008) provide good summaries of such concerns and Petrini *et al.* (2008) make a strong case for the use of *tangent-stiffness-proportional* damping (*tspd*). In the latter formulation $a_M=0$ and the tangent stiffness matrix $\boldsymbol{K}_t$, rather than the initial stiffness matrix, is used:

$$\boldsymbol{C}_t = a_K \boldsymbol{K}_t \tag{3}$$

Charney (2008) argues that this approach still produces spurious damping forces and suggests that also a_K should be periodically updated. Other approaches put forward by researchers are: i) to use Caughey series with $b \leq 0$ (Bernal, 1994); ii) to bind or 'cap' the value of the damping forces; and iii) to model dashpots and non-linear frictional dampers explicitly. This research uses (3) because it is deemed easy to implement and commonly used in practice and research. Due note is made that different results may be obtained with other methods of modelling damping. The damping coefficient is obtained for any desired critical damping ratio ξ_0 at a reference natural period T_0 by solving (2) for a_K with $a_M = 0$:

$$a_K = \xi_0 T_0 \frac{1}{\pi} \tag{4}$$

Table 2 shows how damping changes for each mode and Figure 6 shows values of a_K for T_0=0.62s for different values of reference damping ratio ξ_0. Also shown are the corresponding modal damping ratios at periods other than the reference period to show how higher modes are heavily damped with this approach.

Table 2. Coefficient a_K for T_0=0.62s at selected ξ_0 with corresponding ξ at selected periods

ξ_o [%]	a_K ((4) [s] $\times 10^{-4}$	$\xi_i = a_K \pi T_i^{-1}$ [%]			
		$0.05T_o$	$0.2T_o$	T_o	$2T_o$
		0.03s	0.12s	0.62s	1.24s
0.1	1.97	2	0.5	0.1	0.05
0.5	9.87	10	2.5	0.5	0.3
1	19.7	20	5	1	0.5
2	39.5	40	10	2	1
5	98.7	100	25	5	2.5

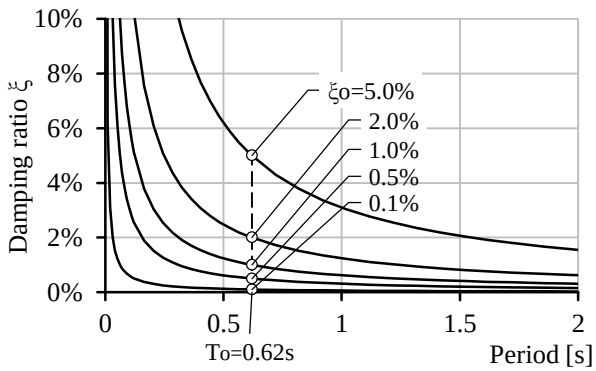

Figure 6.

The damping force vector $\boldsymbol{f}_D$ at any instant is the product of the damping matrix and the nodal velocity vector $\boldsymbol{v}$:

$$\boldsymbol{f}_D(t) = \boldsymbol{C}_t \boldsymbol{v}(t) = a_K K_t \boldsymbol{v}(t) \tag{5}$$

The damping force vector can also be expressed in terms of its modal components for linear systems and for an instantaneous condition of non-linear systems:

$$\boldsymbol{f}_D(t) = \sum_{n-1}^{N} \boldsymbol{f}_{D,n}(t) = a_K \cdot \sum_{n-1}^{N} \frac{4\pi^2}{T_n^2} \cdot \boldsymbol{K}_t \cdot \boldsymbol{\Phi}_n \cdot \dot{\boldsymbol{X}}_n(t) \tag{6}$$

Identifying the Underlying Physical Phenomena

A model ("S") without vertical mass was run with several levels of *tspd* between 0.1% and 5%. The damping matrix was updated at each time step. The axial load variation (ΔN) is seen to clearly depend on the amount of damping in the model (Figure 7, left). The relationship between ΔN and ξ is nearly linear, but not quite, highlighting the dual nature of the effect of damping.

When the same models are run with a pseudo-static cyclic analysis (i.e., with zero velocity and acceleration), the axial load variation disappears ($\Delta N=0$). Furthermore, there does not seem to be any correlation between ΔN and the axial strain ε_0 at the level of the reference axis (Figure 7, right).

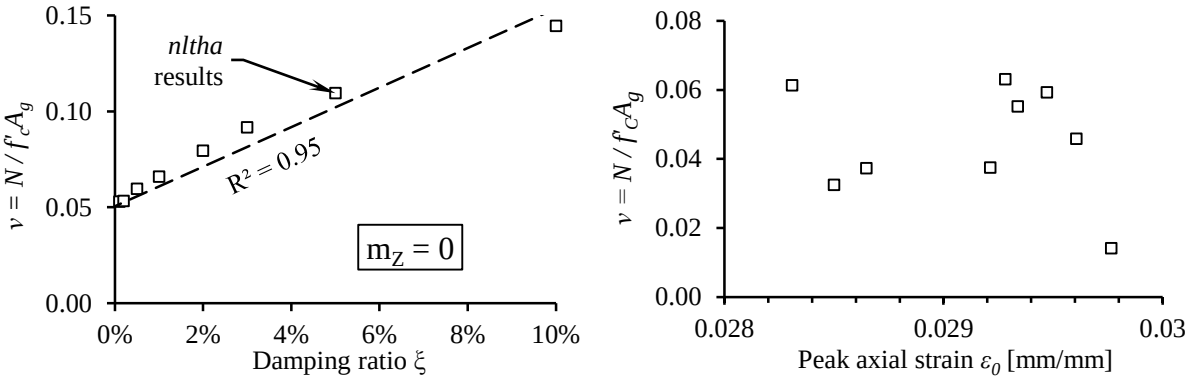

Figure 7. Left: relationship between ΔN and ξ. Right: scatter plot of peak values of ΔN and ε_0. Several runs are shown of models without vertical mass and different values of damping.

When ΔN is plotted together with the vertical velocity of a representative DOF (Figure 8), the time histories nearly match each other, indicating a close correlation between the two. Such correlation is confirmed by plotting ΔN vs vertical velocity as shown on Figure 9 – left. An unbalanced vertical damping force $\boldsymbol{f}_D = \boldsymbol{C} \cdot \boldsymbol{v}_z$ could explain the increment in axial force with correlation coefficients close to unity (0.88 – 0.97). Even though there is no mass in the vertical DOFs there is a non-zero stiffness in the corresponding DOF and since the damping used in this work is stiffness-proportional there is a non-zero damping force.

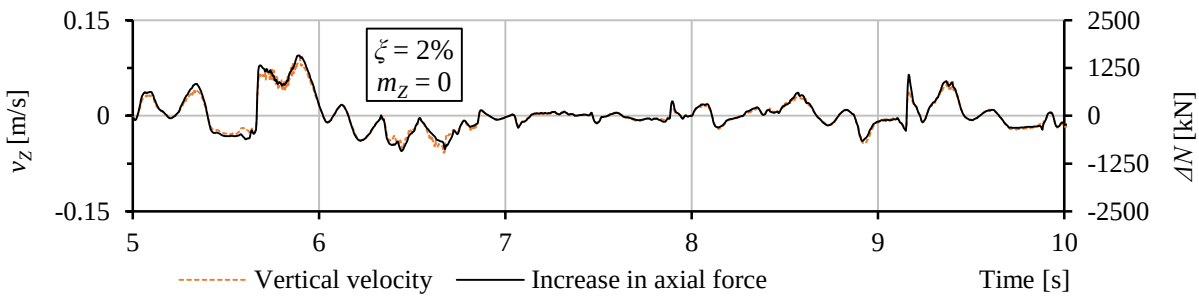

Figure 8. A 5-second-long segment of both ΔN and vertical velocity v_Z are plotted together for the model with 2% damping to illustrate the close match between the two. Model S.

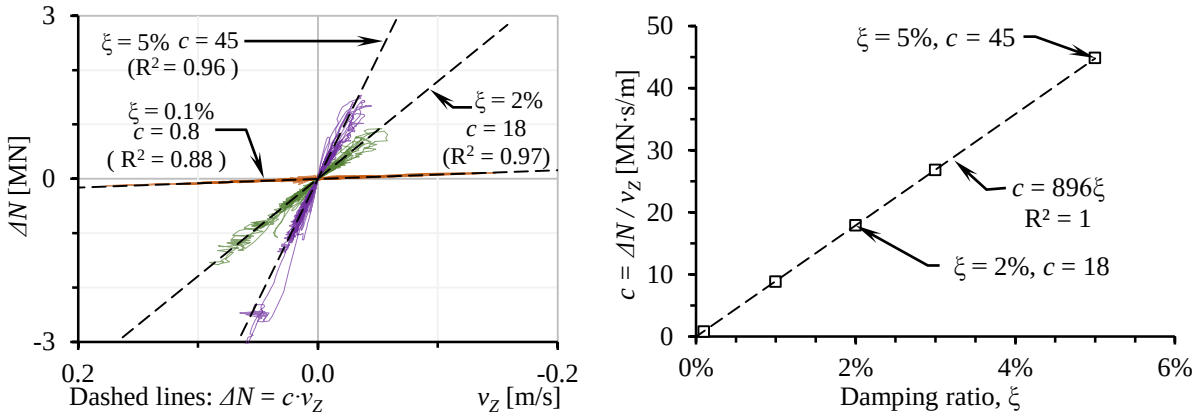

Figure 9. Proportionality between ΔN and v_Z, (left) and between v_Z and ξ (right). Model S. m_z=0.

5. Influence of mass

Effect of modelling a vertical mass

When the same models used to evaluate the effect of damping are run with the vertical mass component activated, it becomes immediately evident that the effect of mass can be much greater than that of damping, as seen in Figure 10. For example, at 2% damping, while the effect of damping accounts for nearly a 50% increase in axial load, the presence of mass nearly trebles the axial load. The relative effect on response parameters relevant to design varies. While the maximum base shear demand can increase significantly, the curvature demand and inter-story drift ratios are not affected as much.

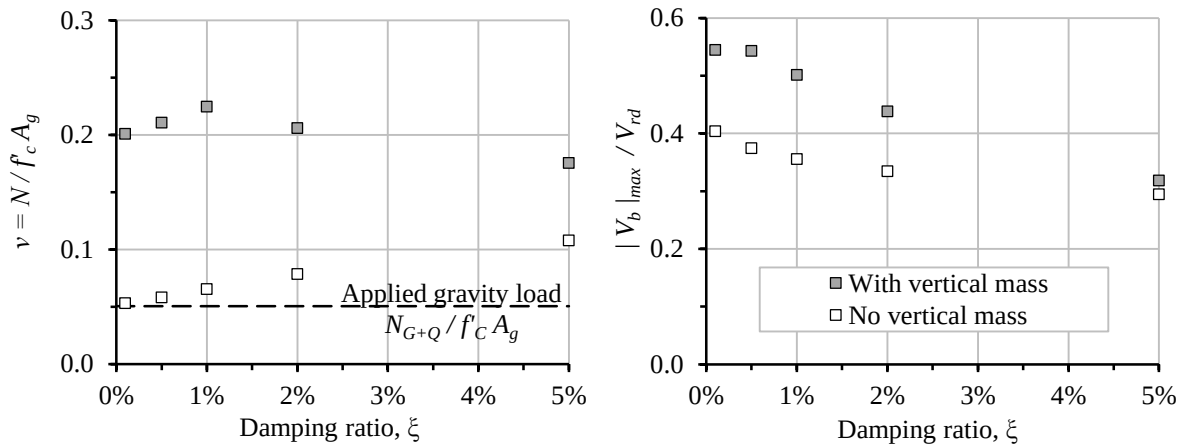

Figure 10. Comparison between models with and without vertical mass in terms of normalized axial force (left) and normalized base shear (right). Note V_{rd} is the shear capacity at wall base per EC8. Model S.

Effect of the amount of vertical mass

The vertical mass in a model can be different to the horizontal mass, among other reasons, because the quantity of interest in this case is the "modal" mass associated with the first-mode vertical response. The mass is distributed over the floor, which has very different stiffness in the in-plane and out-of-plane directions. The vertical mass is carried by the gravity columns as well as by the walls, while the horizontal mass is carried mostly by the walls. To reflect this, several models were run with varying values of the vertical mass.

It was found that the axial load amplification increases with increasing amounts of vertical mass. The presence of mass can mean a 50% increase in predicted base shear with respect to the values assumed for design. The predicted inter-story drift is largely unaffected by this effect. However, the

base shear demand is significantly greater for a system with a large effective vertical mass as compared to one with no vertical mass as shown in Figure 12.

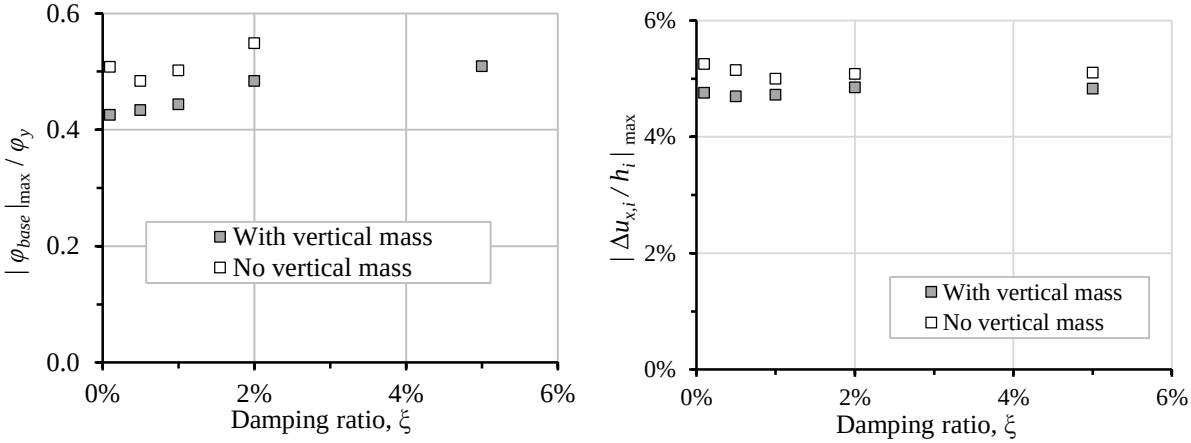

Figure 11. Effect of vertical mass on response. Left: curvature at base. Right: inter-story drift ratio.

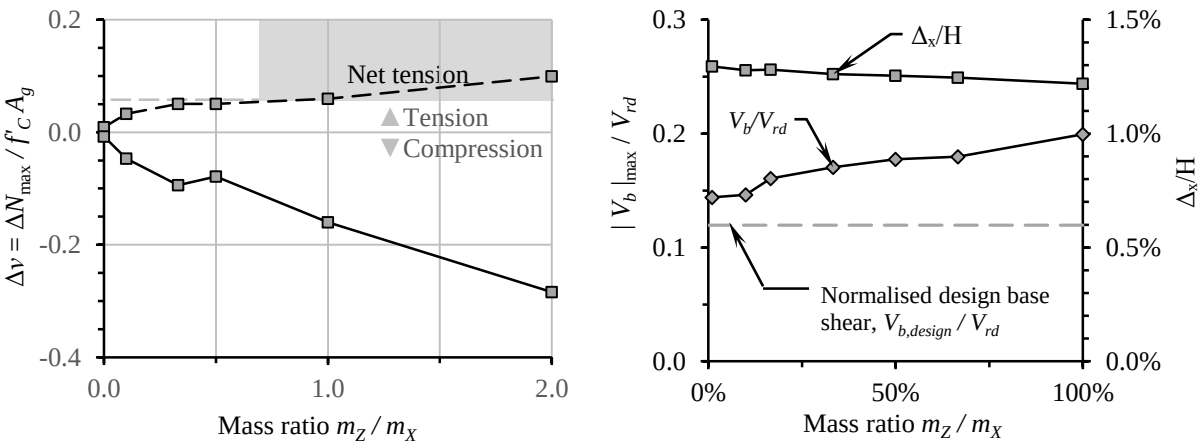

Figure 12. Effect of the amount of vertical mass on the axial force increment (left) and on engineering demand parameters (right). Model S. Values of force are normalized by nominal strength ($f'_c A_g$ and V_{rd}).

Influence of floor system properties

As the out-of-plane properties of the floor system change, so does the effective mass participating in the first-mode vertical response. In general, the increase in axial load will be lower in very flexible floors than in very rigid floors because in the latter the effective vertical mass tends to be closer to 100%. The range of typical floor stiffness (3Hz—12Hz) overlaps with the typical axial stiffness of walls (in this case 10Hz for the first axial mode). This means that the floor system can tune itself with the vertical response of the wall and thus amplify the axial load effect as is apparent in Figure 13. This is also evident in the hysteretic loops of Figure 14 for models with two very different floor stiffness. It shows how very flexible floors (right) lead to small effective vertical mass and thus negligible axial force variation. Conversely, floors with periods close to that of the walls (left) lead to resonance and magnify the effect.

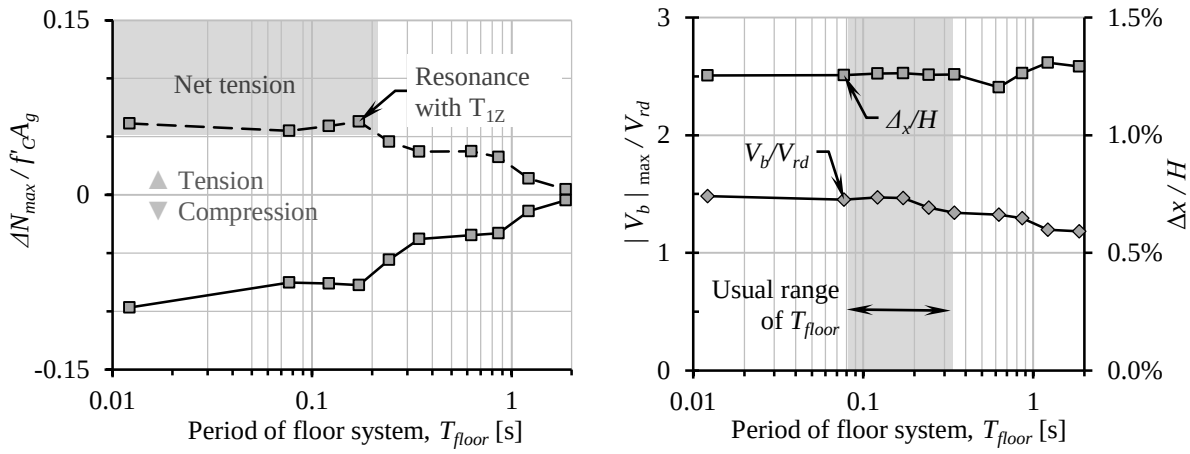

Figure 13. Effect of floor dynamic properties on response: Left: period of the floor system; Right: floor-to-wall vertical stiffness ratio.

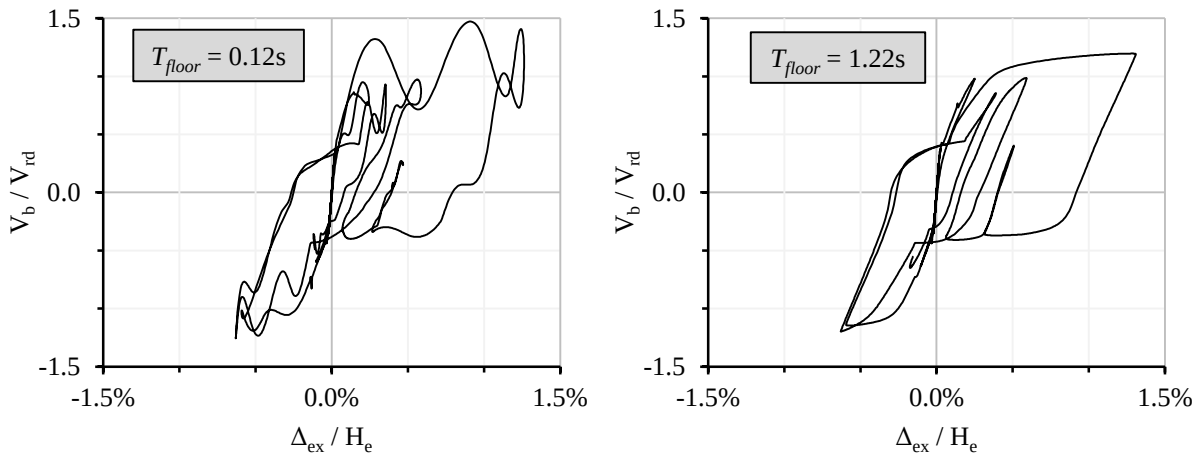

Figure 14. Hysteresis loops with very stiff (left) and very flexible (right) floors in the out-of-plane direction.

6. Conclusions and Future Research

The commonly used stiffness-proportional damping approach can generate spurious damping forces in the axial direction of reinforced-concrete walls modelled with force-based beam elements with fibre sections under non-linear time history analysis. These forces do not represent any real physical phenomenon and thus it is desirable to minimize them by using the lowest possible damping ratio. For models that do include the vertical nodal masses, a case was shown where the inertia forces generated by the dynamic response of the vertical mass coupled with the *rocking-like* motion of the walls cause an increase in the axial forces in the walls. These forces do represent a real physical phenomenon. In both cases, the increase in axial force is a cyclic phenomenon with a much shorter period than the first lateral period of the wall and generates an oscillation of the moment capacity around its theoretical value. This can lead to an increase in base shear demand. Other response parameters such as drift ratio were not as significantly affected, at least in the cases presented in this paper.

Further research is taking place to quantify these effects under different sets of circumstances, such as different reinforcement ratios, wall aspect ratios, levels of axial load and ground motion intensity. This line of research could potentially be carried through to provide recommendations in design codes that allow designers to account for increased base shear demands without the need to use sophisticated non-linear models.

7. References

A.Alipour, F. Z. (2008). Study Rayleigh Damping in Structures: Uncertainties and Treatments. *Proceedings of the 14th WCEE.*

Alipour, A., & Zareian, F. (2008). Study on Rayleigh Damping in Structures: Uncertainties and Treatments. *Proceedings of the 14th WCEE.* Beijing, China.

Bernal, D. (1994). Viscous damping in inelastic structural response. *J. Struct. Eng.*, 120(4):1240–1254.

Charney, F. A. (2008). Unintended Consequences of Modeling Damping In Structures. *J. Struct. Eng.* , 134: 581-592.

Correia, A. A., Almeida, J. P., & Pinho, R. (2013). Seismic Energy Dissipation in Inelastic Frames: Understanding State-of-the-Practice Damping Models. *Structural Engineering International*(2).

Farzin Zareian, R. A. (2010). A practical method for proper modeling of structural damping in inelastic plane structural systems. *Computers and Structures, 88*, 45-53.

Felippa, C. (2013). Retrieved from Course notes for Introduction to Finite Element Methods, Department of Aerospace Engineering Sciences, University of Colorado at Boulder: http://www.colorado.edu/engineering/CAS/courses.d/IFEM.d/Home.html

G. Oliveto, A. G. (2002). Some Observations on the Characterization of Structural Damping. *Journal of Sound and Vibration (2002) 256(3), 391}415*, 256(3): 391-415.

González, A. (2013). *Seismic Demands in Irregular Buildings with Flexible Diaphragms and Self-Centering Dual Frames.* MSc Thesis, ROSE School, Pavia, Italy.

Hall, J. F. (2006). Problems encountered from the use (or misuse) of Rayleigh damping . *Earthquake Engng Struct. Dyn.* , 35:525-545.

Petrini, L., Maggi, C., Priestley, M., & Calvi, G. M. (2008). Experimental Verification of Viscous Damping Modeling for Inelastic Time History Analyzes. *Journal of Earthquake Engineering*, 12(SI):125-145.

Priestley, M., & Grant, D. (2005). Viscous damping in seismic design and analysis. *Journal of Earthquake Engineering*, 9(SI1):229-255.

Richardson, M. H. (n.d.). *Modal Mass, Stiffness and Damping.* Retrieved from Vibrant Technology, Inc., Jamestown, CA: http://www.vibetech.com/assets/papers/paper31.pdf